Int. J. Electrochem. Sci., 16 **(2021)** Article ID: 210664, doi: 10.20964/2021.06.66

International Journal of
ELECTROCHEMICAL
SCIENCE
www.electrochemsci.org

Fabrication of three-dimensional porous Cu current collector for lithium-ion batteries using Space Holder Method

Zhixiang Wang, Deng Pan[*], *Yaqian Liang, Bin Xia, Bingdong Qin, Meng Wang*

School of Materials Science and Engineering, Jiangxi University of Science and Technology, Ganzhou, 341000, China
[*]E-mail: jqpan66@163.com

Received: 31 January 2021 / *Accepted:* 9 April 2021 / *Published:* 30 April 2021

The novel three-dimensional (3D) porous copper was constructed by space holder method based on powder metallurgy technique, which was used as the current collector to develop the high-capacity Sn anode with 3D porous architecture for the lithium-ion batteries. The influences of the porosity of 3D porous copper on the specific capacity and cyclic stability of the Sn anode for lithium-ion batteries were investigated systematically. The results show that the 3D porous Sn-Cu electrode could exhibit relatively higher specific capacity and better cyclic stability compared to the Sn coated Cu foil electrode, and the 3D porous Sn-Cu electrode could maintain better structural integrity after 100 cycles. Especially, when using the copper current collector with porosity of 74.78% to construct the 3D porous Sn-Cu electrode, and the initial specific capacity and coulomb efficiency of electrode could achieve 612.1mAh/g and 71.75%, respectively. Also, it could maintain highest capacity retention ratio of 35.04% after 100 cycles. As a result, this 3D porous copper current collector constructed with space holder method based on powder metallurgy technique could provide an optional approach to improve lithium-ion batteries.

Keywords: Three-dimensional porous Cu; Space holder method; Current collector; Lithium-ion battery

1. INTRODUCTION

Lithium-ion batteries (LIBs) as one of the main power sources play an important role in our daily lives currently， which have been successfully used in many applications such as portable electronic devices, electronic vehicles and large-scale smart girds. With the rapid increase in the performance requirements of these applications for power supplies, it is necessary to develop LIBs with higher specific capacity and better cycling stability than current ones [1-8]. In this case, Sn anode has received a wide attention due to its superior theoretical capacity (994 mAh/g), that is higher than commercial graphite anode [9-16]. However, the intercalation and de-intercalation behaviors of Li^+

will cause huge volume expansion (about 300%) of Sn during the cycles, which can lead to rapid capacity decay and low coulomb efficiency [10, 17-20]. Also, the huge volume expansion could result in continuous solid electrolyte interphase (SEI) films during the cycles, which might cause pulverization and loss of electrical contact at the electrode, and it even causes the danger of battery explosion. Constructing 3D porous current collectors could be considered an effective way to solve those problems for LIBs. Because this architecture can not only restrict the severe volume expansion inside the anode, but also provide a larger specific surface area to enhance the electrochemical reactions [21-26].

Li and Hu et al [22] reported a commercial copper foam as current collector to fabricate 3D porous Sn-Cu electrodes via electrolessly plated Sn layer, and it focused on the effect thickness of Sn layer on specific capacity and cyclic stability, indicating that the 3D porous architecture can restrict severe volume changes of Sn during the process of charging and discharging. Luo and Xu et al [24] fabricated 3D porous Sn-Cu electrodes by a combination of molten-metal infiltration and de-alloying as well as electroless plating, and it showed that this type of electrodes with 3D porous Sn-Cu architecture could exhibit higher specific capacity and better cyclic stability compared to the planar Sn-Cu electrodes. Recently, Park and Um et al [25] proposed a combination of freeze-casting and electroless plating to construct 3D porous Sn-Cu electrodes, which had a more positive effect on the improvement of specific capacity and cycling. Besides, Wang and Yin et al [27] used laser micro-processing to construct 3D porous architecture to stable Li metal anodes while the high cost or inefficient process limited its application.

The space holder method could be considered as a low-cost and easy technique, especially, it could possess the characteristics of better mechanical properties, controllable structure and adjustable porosity for constructing 3D porous current collectors [28,29]. In present study, three-dimensional (3D) porous copper with different porosities was constructed by space holder method based on powder metallurgy technique, and then electrolessly plated a layer of Sn on porous copper current collector so as to fabricate 3D porous Sn-Cu electrodes. The electrochemical performances and structural characterization of 3D porous Sn-Cu electrodes were investigated systematically, and it found that the 3D porous Sn-Cu electrode could exhibit relatively higher specific capacity and better cyclic stability. Thereby, this 3D porous copper current collector constructed with space holder method based on powder metallurgy technique could provide an optional approach to improve lithium-ion batteries.

2. EXPERIMENTAL

2.1. The preparation of electrodes

3D porous Cu current collectors were constructed by the space holder method based on powder metallurgy technique Firstly, the spherical K_2CO_3 was selected for space holder, and then the pure electrolytic Cu powder was selected for metal powder. The pure Cu powders were mixed with 40, 50, 60, 70, 80 vol.% of space holders, respectively, in a planetary ball mill, and also the ethanol was added into the mixture in order to better combine the copper powders and the space holders. Then, the

mixture was poured into a cylindrical steel mold, which was compacted in one direction at 200 MPa under a hydraulic press and kept for 30 s to obtain precursor. Subsequently, the precursor was sintered at 850℃ for four hours under flowing argon atmosphere in a tube furnace. At last, the precursor was rinsed in running boiling water to dissolve the space holder to obtain porous Cu framework. The as-fabricated precursor was cut into $10\times10\times1$ mm^3 slice to form 3D porous Cu current collector. Herein, the current collector with 40, 50, 60, 70, 80 vol.% of space holder were named S1, S2, S3, S4, S5, respectively. Meanwhile, the 3D porous Cu current collector was immersed in electroless tin plating solution at room temperature for 3min to fabricate 3D porous Sn-Cu electrodes. The electrodes used 3D porous Cu current collector with 40, 50, 60, 70, 80 vol.% of space holders were named S1/Sn, S2/Sn, S3/Sn, S4/Sn, S5/Sn, respectively. Besides, we fabricated a Sn electrode used copper foil as the current collector as the reference sample named S0/Sn with the same electroless plating process. The manufacturer of the electroless tin plating solution was Weihai Yunqing Chemical Industry Research Institute. The Cu powder was purchased from Beijing Xingrongyuan Technology Co., Ltd. The space holder was purchased from Xilong Chemical Co., Ltd.

2.2. The characterization of electrodes

The MLA650F-type scanning electron microscope was used for microstructure observation. The porosity of the sample was measured by the Archimedes drainage method, and the porosity can be calculated by Eq. (1) where P stands for porosity, ρ and ρ_s are the density of 3D porous copper and pure copper, respectively.

$$P\,(\%)=1-\frac{\rho}{\rho_s}\times100 \qquad (1)$$

The universal testing machine was used to investigate the mechanical behavior of samples with different porosity. In order to explore the phase transition during the preparation process, we used the Empyrean X-ray diffractometer to analyze the phase composition of the samples. Also, the elements of the samples were analyzed by EDS. CR2032-type coin cells were assembled in a glove box. A slice of lithium metal was used as cathode, and the sample was used as the anode. The type of separator was Celgard2300, and the electrolyte solution was $LiPF_6$ in EC-DEC (volume ratio 1:1) with 1 mol/L. The charge/discharge cycling behavior was tested at a current density of 50 mA/g between 0.01-2.00V (vs Li/Li^+) in the LandCT2001A test system. The cyclic voltammetry behavior was tested in the CHI660E electrochemical workstation with a sweep rate of 0.1mV/s.

3. RESULTS AND DISCUSSION

3.1. Morphology and structure

Fig. 1(a) shows the porosities of 3D porous Cu current collectors with different volume fractions of space holders constructed by the space holder method based on powder metallurgy technique. In general, the porosity of the 3D porous Cu current collector was higher than that of its corresponding volume fraction of space holders, which was due to the combination of metal powders

to form extra pores during the sintering process. As a result, when the volume fractions of space holders were 40%, 50%, 60%, 70% and 80%, the corresponding porosities of as-fabricated samples were 48.21%, 58.01%, 66.86%, 74.78% and 81.65%, respectively. The porosity could increase along with the volume fraction of space holder, so we can adjust the volume fraction of the space holder to adjust the porosity of the 3D porous architecture through the space holder method. Fig. 1(b) shows the stress-strain curves of 3D porous Cu current collectors, it can be seen that the plateau stress gradually decreased from S1 to S5, indicating that the mechanical property of as-fabricated samples would deteriorate with the increase of the porosity. Because the pore wall of high-porosity sample was thinner compared to the low-porosity sample, it could make worse for the resistance to deformation. The results were similar to those previously reported by Zhao and Fung et al [30]. Comparing with the Cu foam current collector [22], the porosity of as-fabricated 3D porous Cu current collector could be adjusted. Comparing with the Cu current collector of oriented pore structure obtained using the freeze-casting process [25], it could have much higher open porosity via the porous architecture of the spherical pores fabricated by space holder method, which would make the stress distribution uniform and promotes the interface contact between the electrode and the electrolyte. Besides, the fabricating process could be cheaper and simpler comparing with the 3D Cu current collector fabricated by laser micro-processing [27].

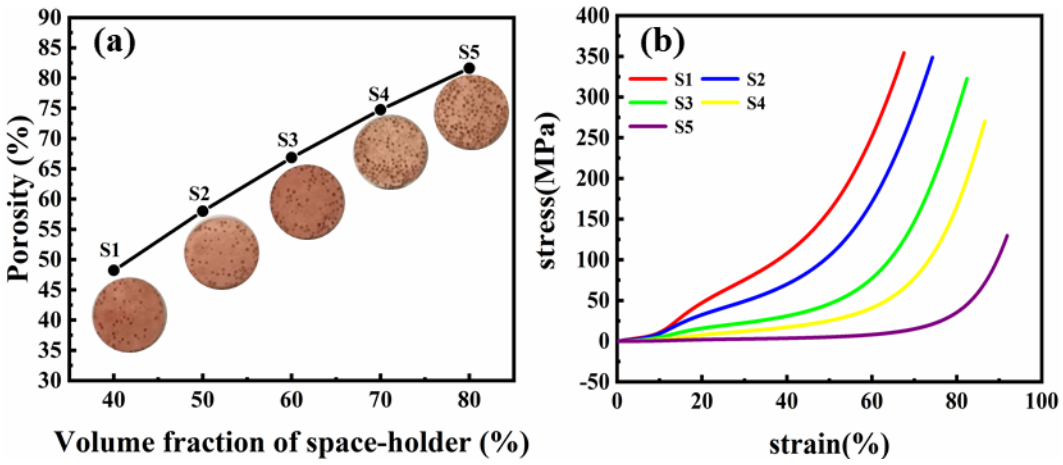

Figure 1. (a) The porosities of 3D porous Cu current collectors (S1-S5) with different volume fractions of space holders and (b) stress-strain curves of 3D porous Cu current collectors (S1-S5) with different volume fractions of space holders, S1: 40 vol.%; S2: 50 vol.%; S3: 60 vol.%; S4: 70 vol.%; S5: 80 vol.%.

Fig. 2 shows the representative photographs and SEM images of the 3D porous Sn-Cu electrodes with different current collectors. The representative photographs show that the pores were evenly distributed in the electrodes, and the distribution of pores changed from sparse to dense as the volume fraction of the space holders increased. As shown from the corresponding SEM images, the electrodes displayed the spherical pores caused by dissolution of the space holders. At the same time, there were much smaller spherical pores caused by the combination of metal powders during the sintering process. It found that defects appeared gradually around the large hole as the volume fraction of the space holder increased (Fig 2(c), (d), (e)), which was due to the gradual uneven filling of the

metal powders in the gaps between the space holders during the mixing. When the volume fraction of space holder reached 80 % (Fig 2(e)), the electrode presented the most defects. Besides, the square Sn particles can be seen clearly on the electrodes from the high magnification SEM images, and even they could be uniformly distributed on the surface of the pore walls.

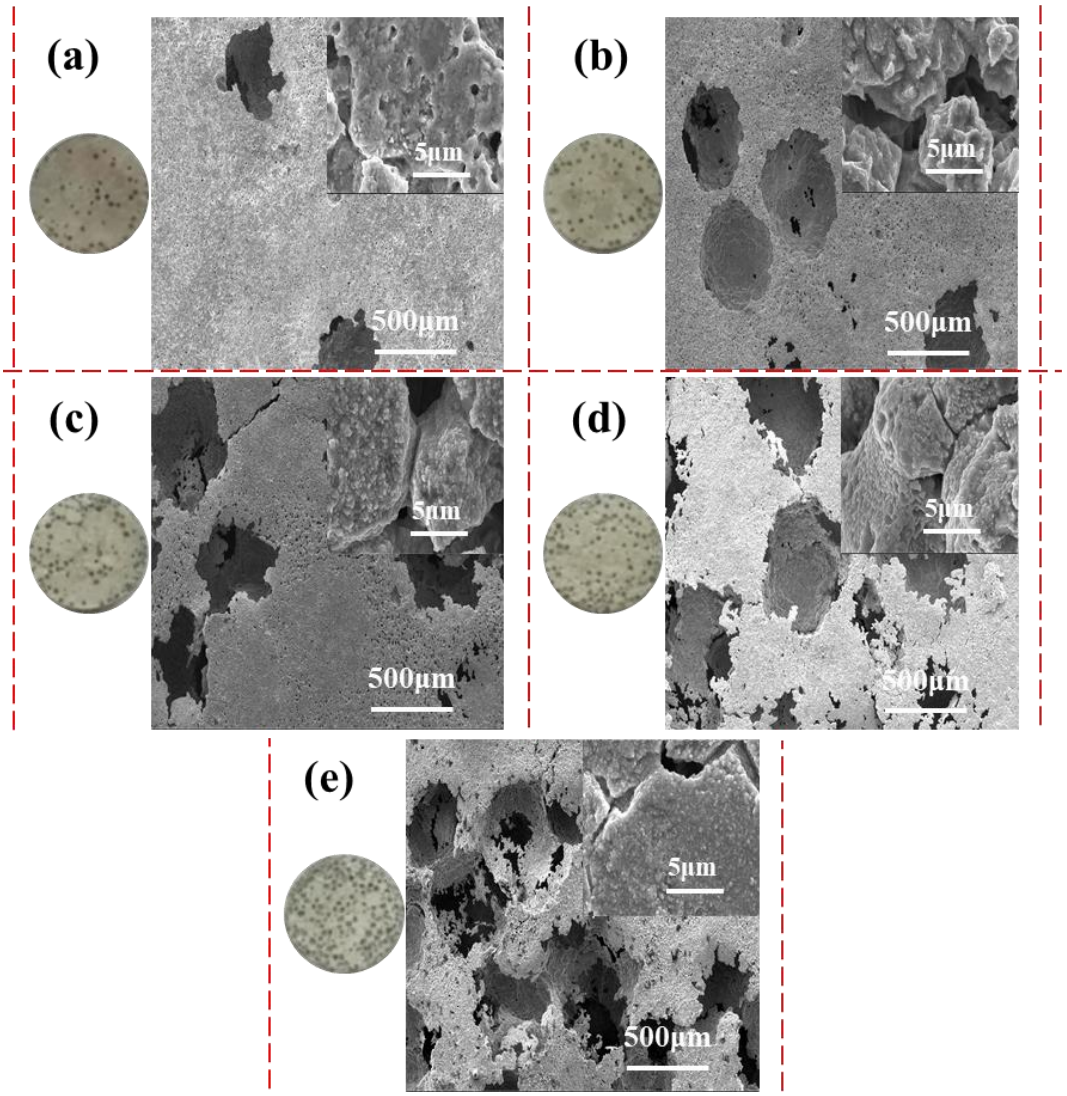

Figure 2. The representative photographs and SEM images of 3D porous Sn-Cu electrodes (S1/Sn-S5/Sn) using different current collector with different volume fractions of space holders, (a) S1/Sn: 40 vol.%; (b) S2/Sn: 50 vol.%; (c) S3/Sn: 60 vol.%; (d) S4/Sn: 70 vol.%;(e) S5/Sn: 80 vol.%.

Fig. 3(a) shows XRD patterns of 3D porous Cu before (I) and after (II) electroless plating of Sn, it can be seen from (I) that there are only characteristic diffraction peaks of Cu phase, indicating that the space holder (K_2CO_3) did not react with Cu during the sintering process and the space holder was removed cleanly after dissolving. The characteristic peaks of O were not found, revealing that the 3D porous Cu was not oxidized during the sintering or the oxide might be beyond the detection accuracy of XRD. (II) shows that the characteristic diffraction peaks of Sn and Cu_6Sn_5 phases appeared after electroless plating of Sn, indicating that Cu_6Sn_5 intermetallic compound was formed during

electroless plating. And, the 3D porous Cu after electroless plating of Sn was a Sn-Cu_6Sn_5 composite electrode. Fig. 3(b) shows the energy dispersive spectrogram (EDS) of the 3D porous Cu-Sn electrode, it mainly presented two characteristic peaks of Cu and Sn. Besides, there was weak peak of O, which was due to slight oxidation when drying the sample.

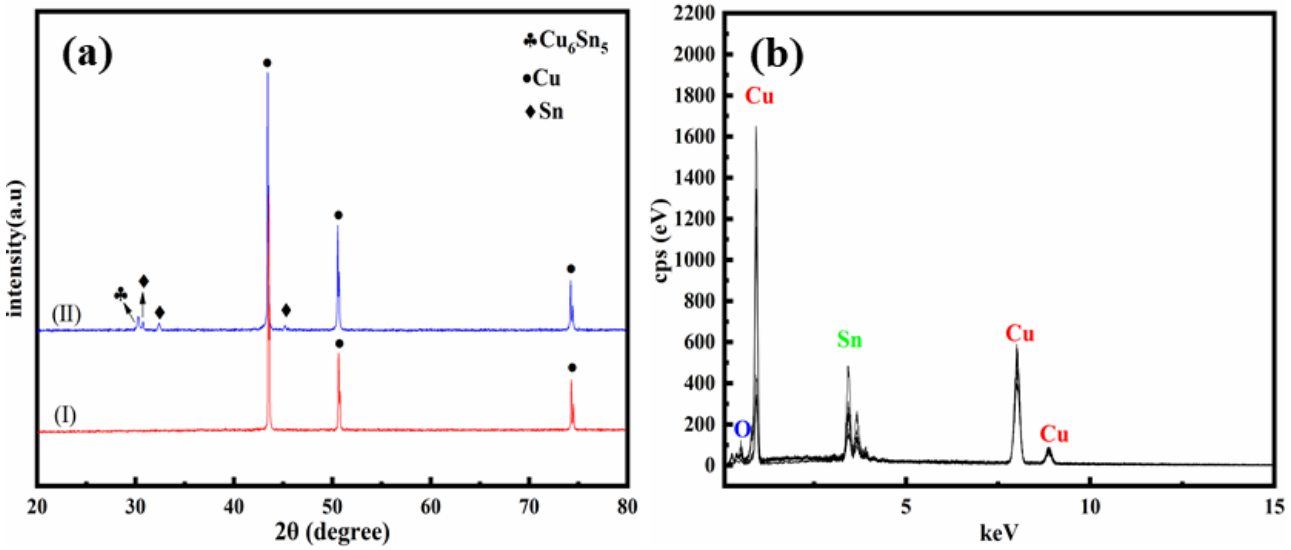

Figure 3. XRD patterns of (a) 3D porous Cu electrode before (I) electroless plating of Sn and after (II) electroless plating of Sn; and EDS spectrogram of (b) 3D porous Sn-Cu electrode.

3.2. Electrochemical performance

In order to investigate the reactive process of the 3D porous Sn-Cu electrode, the cycling voltammetry (CV) of the 3D porous Sn-Cu electrode was conducted for three cycles in the voltage range of 0.01-2 V at a scanning speed of 0.1mV/s. As shown in Fig. 4, at the first Lithium insertion process (1st cycle), the weak reduction peak near 0.65 V were corresponded to the formation of Li_xSn alloy, as shown in Eq. (2) [22]. In addition, it can be clear found that there were the reduction peaks near 0.33 V and 0.15 V, corresponding to phase transitions of Eq. (3) and Eq. (4), respectively [31, 32]. And, the reduction peaks near 0.24V were corresponded to the Eq. (2) [25] during the 2nd and 3rd.

$$x\mathrm{Li}^+ + \mathrm{Sn} + x\mathrm{e}^- \rightleftharpoons \mathrm{Li}_x\mathrm{Sn} \quad (2)$$

$$10\mathrm{Li}^+ + \mathrm{Cu}_6\mathrm{Sn}_5 + 10\mathrm{e}^- \rightleftharpoons 5\mathrm{Li}_2\mathrm{CuSn} + \mathrm{Cu} \quad (3)$$

$$12\mathrm{Li} + 5\mathrm{Li}_2\mathrm{CuSn} \rightleftharpoons 5\mathrm{Li}_{4.4}\mathrm{Sn} + 5\mathrm{Cu} \quad (4)$$

In the process of retrace voltage, there were three distinct oxidation peaks near 0.54V, 0.63V and 0.83V, and the corresponding process was lithium ions de-intercalation. The oxidation current peaks displayed at 0.54, 0.63 and 0.83V were basically similar within 3 cycles. The peak values of 1st were roughly similar with the initial charge and discharge curves. Also, those similar CV behaviors were reported by Park and Um et al [22] and Li and Hu et al [25].

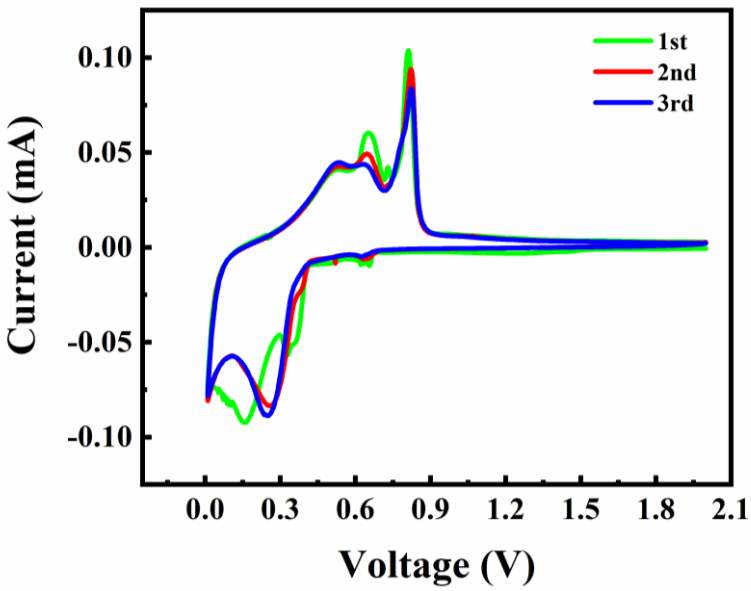

Figure 4. Cyclic voltammogram curves of 3D porous Sn-Cu electrode.

Fig. 5(a) shows the initial charge and discharge curves of the electrodes in the voltage range of 0.01-2 V at a current density of 50 mA/g, the discharge curves of the electrodes presented two plateaus around 0.3 V and 0.15 V, and the result was consistent as reported by Xue and Fu et al [33]. The two plateaus were corresponding to the transition of Cu_6Sn_5 into Li_2CuSn phase (Eq. (3)) and the transition of Li_2CuSn into $Li_{4.4}Sn$ phase (Eq. (4)). It found that the initial discharge specific capacity of S1/Sn-S5/Sn increased sequentially, indicating that the larger porosity of the current collector, the more helpful for increasing the specific capacity of the electrode. In particular, the initial discharge specific capacities of S1/Sn-S5/Sn were significantly higher than that of S0/Sn, indicating that the 3D porous Cu architecture could have an advantage in lithium storage. Moreover, S5/Sn exhibited highest initial discharge specific capacity with 989.2mAh/g. As shown in Fig. 5(b), it can be seen that the initial coulomb efficiency (ICE) of S0/Sn-S5/Sn increased sequentially, and the ICEs of S0/Sn, S1/Sn, S2/Sn, S3/Sn, S4/Sn and S5/Sn were 31.56%, 39.02%, 62.78%, 64.41%, 71.75% and 73.62%, respectively, and thereby S5/Sn could possess the highest ICE of 73.62%. Fig. 5(c) exhibit the cycling performances of S0/Sn-S5/Sn, it can be seen that S4/Sn could have the most stable specific capacity, while the specific capacity of S5/Sn dropped rapidly at the 70th cycles. As shown in Fig. 5(d), the capacity retention ratio of S0/Sn-S5/Sn increased first and then reversed, the capacity retention ratios of S0/Sn-S5 were 20.71%, 24.13%, 33%, 33.53%, 35.04% and 19.04%, respectively. In particular, S4/Sn electrode showed the best cycling stability with a capacity retention ratio of 35.04%, which could provide a discharge specific capacity of 298.9mAh/g after 100 cycles. However, S5/Sn showed the lowest capacity retention ratio, its discharge specific capacity was only 19.04% after 100 cycles. The increased ICE and capacity retention ratio should be attributed to the increase of porosity that could be better to adjust the structural strain caused by the growth of Sn particles during cycling. Besides, the obvious deterioration of the cycling stability of S5/Sn should be due to the excessively high porosity.

Because much higher porosity would cause the deterioration of the mechanical properties of the 3D porous Sn-Cu electrodes so that it cannot support the internal stress caused by the growth of Sn particles during charge and discharge, as a result, it could cause much more damage to the electrode.

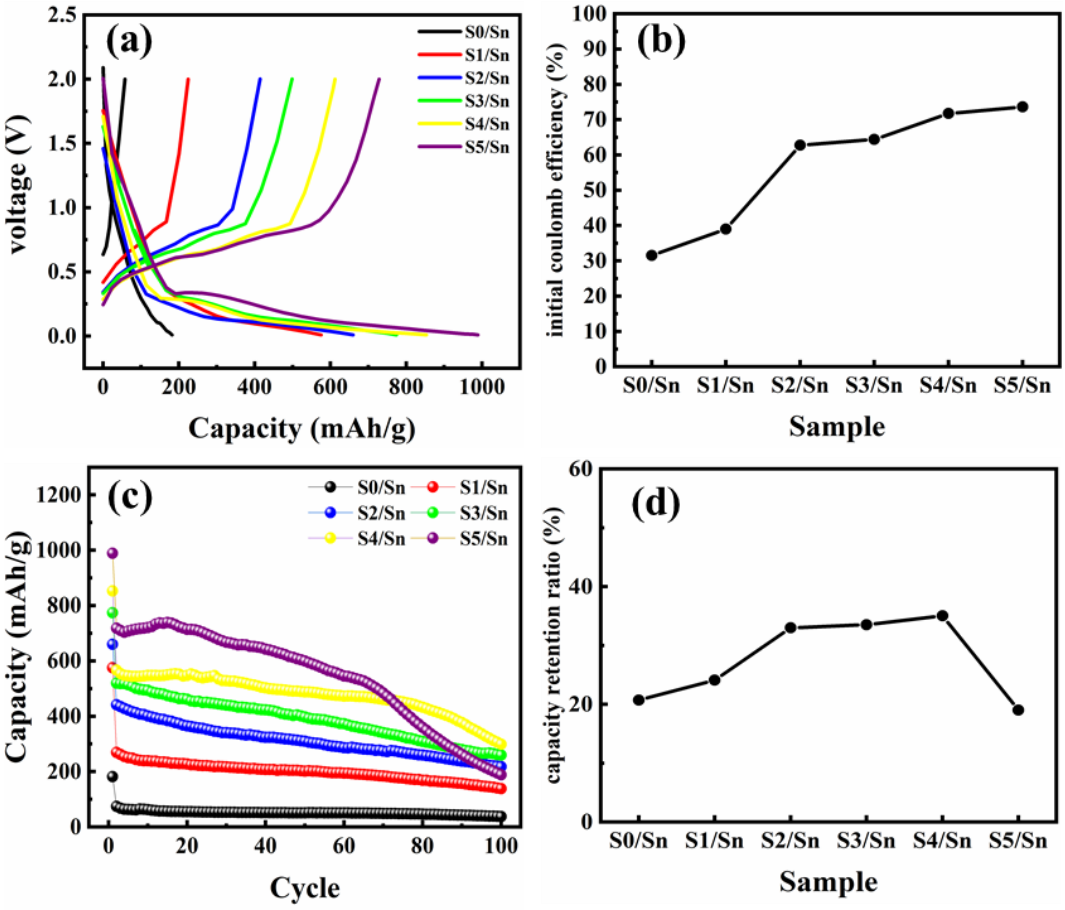

Figure 5. (a) The first charge-discharge profiles and (b) ICEs of electrodes and (c) the cycling performances of electrodes and (d) the capacity retention ratio of electrodes, S0/Sn: Sn-coated Cu foil electrode; S1/Sn-S5/Sn: 3D porous Sn-Cu electrodes using current collectors with different volume fractions of space holders (S1/Sn:40 vol.%; S2/Sn: 50 vol.%; S3/Sn: 60 vol.%; S4/Sn: 70 vol.%; S5/Sn: 80 vol.%).

In order to verify the change for the architecture of the 3D porous Sn-Cu electrodes after 100 cycles, the batteries were disassembled after 100 cycles to take out the electrodes so as to observe their microstructure. As shown in Fig. 6, it can be found that the surfaces of the electrodes were covered with the active material after cycling, and there were a few cracks on the surface of electrodes caused by the volume change of Sn particles during cycling. Besides, the volume change of Sn particles caused stress to squeeze the pore wall, which would make it to deform. Whereas, the pore walls of S1/Sn (Fig. 6(a)) and S2/Sn (Fig. 6(b)) maintained the original shape due to their relatively better mechanical properties of current collectors. As the porosity increased, the pore walls of 3D porous architecture gradually became thinner and the mechanical properties of 3D porous architecture gradually deteriorated, which would result in the resistance to deformation and gradually deteriorated during cycling. The deformation occurred at the thin pore wall of S3/Sn (Fig. 6(c)) and S4/Sn (Fig.

6(d)). When the porosity of S5 reached to 81.56%, the pore walls of S5/Sn (Fig. 6(e)) fractured after cycling, and then it would cause poor cycling stability.

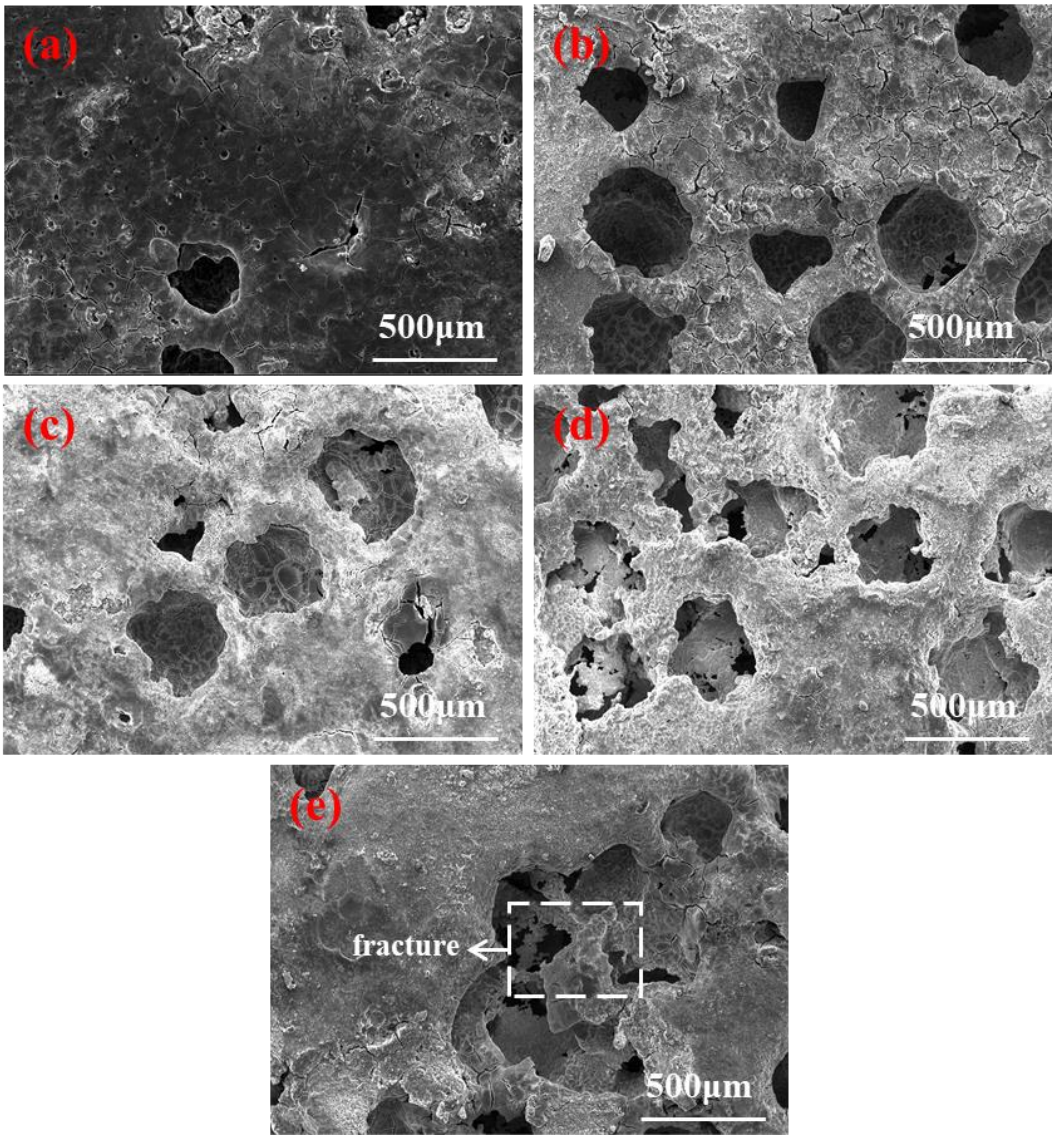

Figure 6. SEM images of 3D porous Sn-Cu electrodes using current collectors with different volume fractions of space holders after 100 cycles, (a) S1/Sn: 40 vol.%; (b) S2/Sn: 50 vol.%; (c) S3/Sn: 60 vol.%; (d) S4/Sn: 70 vol.%;(e) S5/Sn: 80 vol.%.

The volume change of the Sn particles of the Sn-coated Cu foil electrode and the 3D porous Sn-Cu electrode after cycling is shown in the Fig. 7(a) and Fig. 7 (b). For Sn-coated Cu foil electrode, it could clearly found the raised Sn particles on the surface after cycling, which would result in relatively poor ICE and cyclic stability. However, when the Sn particles grew into the pores and grooves of 3D porous Sn-Cu electr ode, there were no obvious raised Sn particles on the surface. Based on the results of SEM images, we simulated the volume change of the Sn on the surface of Sn-coated Cu foil electrode (Fig. 8(a)) and the 3D porous Sn-Cu electrode (Fig. 8(b)). For the Sn-coated Cu foil electrode, Sn particles grew vigorously on the surface after cycling, indicating that 2D planar

architecture cannot limit the volume change of Sn particles during cycling. For the 3D porous Sn-Cu electrode, the 3D porous architecture could provide space for the growth of Sn, and thereby the structure change was smoother compared to the 2D plane architecture after cycling.

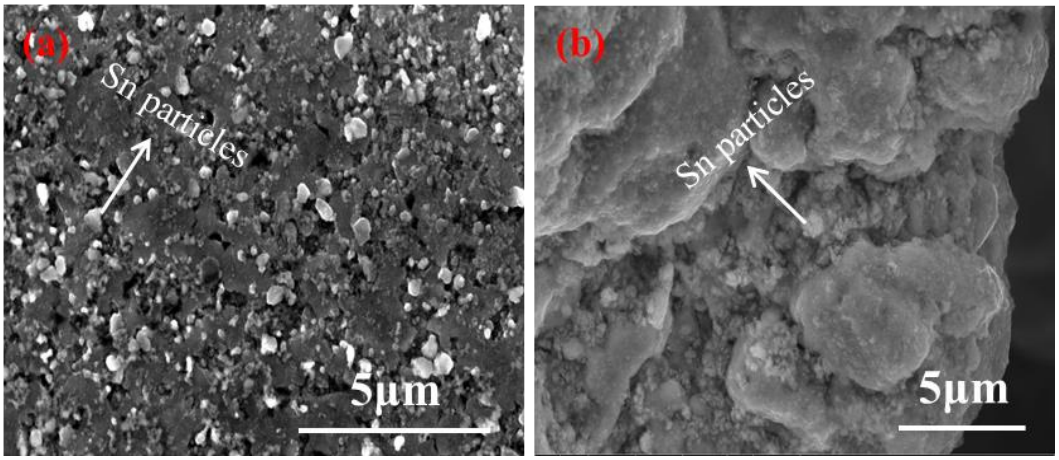

Figure 7. SEM images of Sn particles on the surface of (a) Sn-coated Cu foil electrode and (b) 3D porous Sn-Cu electrode after cycling.

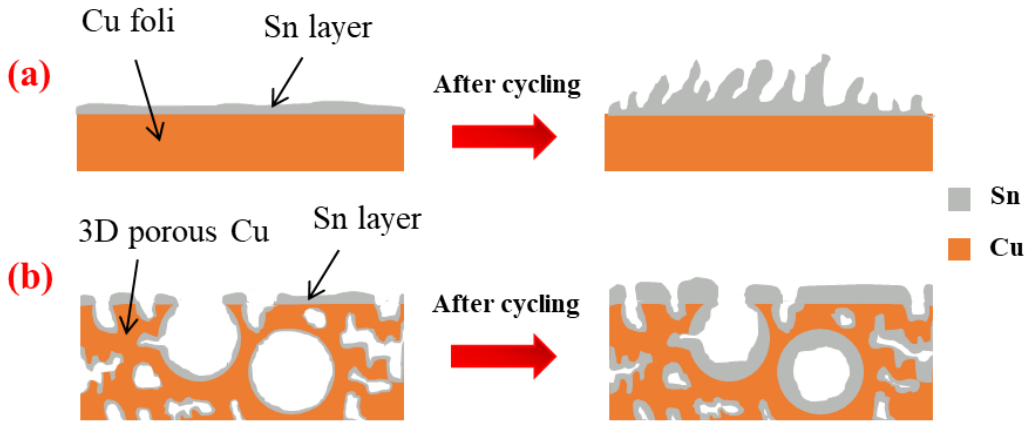

Figure 8. The schematic illustrations of Li deposition on (a) Sn-coated Cu foil electrode and (b) 3D porous Sn-Cu electrode.

4. CONCLUSIONS

The 3D porous Cu current collector was successfully constructed by the space-holder technique based on powder metallurgy technique, and they were used to develop the high-capacity Sn anode with 3D porous architecture for the lithium-ion batteries. The as-fabricated 3D porous Sn-Cu electrode could exhibit relatively higher specific capacity and better cyclic stability. The electrochemical performances of 3D porous Sn-Cu anode would be varied with the increase of the porosity of 3D

porous Cu current collector. Remarkably, the 3D porous Sn-Cu electrode could possess relatively high initial specific capacity and coulomb efficiency as well as highest specific capacity retention ratio when using the copper current collector with porosity of 74.78%. However, the excessively high porosity resulted in poor mechanical properties of the 3D porous Cu current collector, and it would arouse the worse cycling stability of electrode. Therefore, this 3D porous copper current collector with optimum porosity could achieve better combined performances for lithium-ion batteries.

ACKNOWLEDGEMENTS
This work was jointly supported by the Youth Jinggang Scholars Program in Jiangxi Province and the Program for Excellent Young Talents, JXUST (JXUSTQJBJ2016011).

References

1. J.W. Choi, D. Aurbach, *Nat. Rev. Mater.,* 1 (2016) 16013.
2. R. Fang, K. Chen, L. Yin, Z. Sun, F. Li , H.M. Cheng, *Adv. Mater.*, 31 (2019) 1800863.
3. G. Wang, J. Zhang, S. Yang, F. Wang, X. Zhuang, K. Müllen, X. Feng, *Adv. Energy Mater.,* 8 (2018) 1702254.
4. M. Li, J. Lu, Z. Chen, K. Amine, *Adv. Mater.*, 30 (2018) 1800561.
5. X. Li, X. Sun, X. Hu, F. Fan , G.D. Stucky, *Nano Energy.*, 77 (2020) 105143.
6. N. Nitta, F. Wu, J.T. Lee, G. Yushin, *Mater. Today.,* 18 (2015) 252.
7. Q. Xu, J.Y. Li, J.K. Sun, Y.X. Yin, L.J. Wan , Y.G. Guo, *Adv. Energy Mater.*, 7 (2017) 1601481
8. X. Yang, H. Ma, G. Zhang, X. Li, *Adv. Mater. Interfaces.*, 6 (2019) 1801809.
9. H. Tian, F. Xin, X. Wang, W. He, W. Han, *J. Materiomics.*, 1 (2015) 153.
10. B. Fan, J. Liu, Y. Xu, Q. Tang, Y. Zhang, X. Chen , A. Hu, *J. Alloys Compd.*, 857 (2020) 157920.
11. Y. Feng, K. Wu, H. Dong, X. Huang, M. He, *Colloids Surf., A.,* 602 (2020) 125069.
12. J. Zeng, C. Peng, R. Wang, C. Cao, X. Wang, J. Liu, *Powder Technol.,* 364 (2020) 719.
13. X. Li, C. He, J. Zheng, W. Ye, Y. Rui, *J. Alloys Compd.*, 842 (2020) 155605.
14. X Zhang, C Wang, X Dong, J Liang, D Gao. W. Yang, Z. Zhang, *J. Solid State Chem.*, 290 (2020) 121534.
15. H. Zhao, W. Yuan, G. Liu, *Nano Today*, 10 (2015) 193.
16. Z. Jin, L. Ben, H. Yu, W. Zhao, X. Huang, *Prog. Nat. Sci.: Mater. Int.*, 30 (2020) 456.
17. J.Y. Huang, L. Zhong, C.M. Wang, J.P. Sullivan, W. Xu, L.Q. Zhang, J. Li, *Science,* 330 (2011) 1515.
18. S. Kang, X. Chen, J. Niu, *Nano Lett.*, 18 (2018) 467.
19. D. Liu, Z.J. Liu, X. Li, W. Xie, D. He, *Small*, 13 (2017) 170200.
20. L. Sun, X. Wang, R.A. Susantyoko, Q. Zhang, *Carbon*, 82 (2015) 282.
21. X.Y. Fan, Y.X. Shi, J.J. Wang, J. Wang, X.Y. Shi, L. Xu, L. Gou , D.L. Li, *Solid State Ionics.,* 237 (2013) 1.
22. Q. Li, S. Hu, H. Wang, F. Wang, X. Zhong, X. Wang, *Electrochim. Acta.*, 54 (2009) 5884.
23. D.H. Nam, R.H. Kim, W.H. Dong, H.S. Kwon, *Electrochim. Acta.*, 66 (2012) 126.
24. Z. Luo, J.C. Xu, B. Yuan, H. Li, R.Z. Hua, L.C. Yang, Y. Gao, M. Zhu, *Mater. Lett.*, 213 (2018) 189
25. H. Park, J.H. Um, H. Choi, W.S. Yoon, Y.E. Sung, H. Choe, *Appl. Surf. Sci.*, 399 (2016) 132.
26. S. Wang, W. Zhao, Y. Wang, X. Liu, L. Li, *Electrochim. Acta.*, 109 (2013) 46.
27. S.H. Wang, Y.X. Yin, T.T. Zuo, W. Dong, J.Y. Li, J.L. Shi, C.H. Zhang, N.W. Li, C.J. Li, Y.G. Guo, *Adv. Mater.*, 29 (2017) 1703729.
28. H. Fan, Q. Dong, C. Gao, B. Hong, Y. Lai, *Mater. Lett.*, 234 (2019) 69.

29. N. Tuncer, M. Bram, A. Laptev, T. Beck, A. Moser, H.P. Buchkremer, *J. Mater. Process. Technol.*, 214 (2014) 1352.
30. Y.Y. Zhao, T. Fung, L.P. Zhang, F.L. Zhang, *Scr. Mater.*, 52 (2005) 295.
31. D. Larcher, L.Y. Beaulieu, D.D. MacNeil, J.R. Dahna, *J. Electrochem. Soc.*, 147 (2000) 1658.
32. L. Fransson, E. Nordström, K. Edström, L. Häggström, M.M. Thackeray, *J. Electrochem.Soc.*, 149 (2002) A736.
33. L. Xue, Z. Fu, Y. Yao, T. Huang, A. Yu, *Electrochim. Acta.*, 55 (2010) 7310.